EXPANSION DUE TO COMPRESSION TESTS FOR RIA SITUATIONS

A. ZOUARI[1, 2], M. BONO[1], D. LE BOULCH[1], T. LE JOLU[1], J. BESSON[2], J. CREPIN[2]

[1]*CEA Saclay/DEN/DANS/DMN/SEMI, 91191 Gif-sur-Yvette, France*
[2]*Mines ParisTech/Centre des materiaux 7633, 91003 Evry, France*

Expansion Due to Compression (EDC) tests were conducted in order to reproduce the mechanical conditions during the low temperature phase of a power transient in a reactor, also called the Pellet Cladding Mechanical Interaction (PCMI) phase. The tests are intended to reproduce, as closely as possible, the loading mode and macroscopic failure aspects that have been observed during integral RIA tests performed on fuel rods. Different kinds of EDC tests with varying stress biaxiality conditions have been performed in order to study the evolution of the circumferential strain at failure as a function of the strain biaxiality. Three EDC configurations are tested with different values of biaxiality. For each method, the strain field in the sample is measured using a stereo-correlation image analysis technique. The tests show that the hoop strain at failure tends to decrease as the strain biaxiality ratio increases. The experimentally measured hoop and axial strains are in close agreement with finite element simulations performed using CAST3M.

1. Introduction

In order to verify the integrity of fuel rods during Reactivity Initiated Accidents (RIA) in Pressurized Water Reactors (PWR), many types of experimental tests have been developed to evaluate the mechanical behavior of the cladding (1) (2). A RIA caused by the uncontrolled ejection of a control rod is presumed as one of the design basis accidents for PWRs. During the first phase of a RIA, the zirconium alloy fuel cladding tubes may be subjected to Pellet-Cladding Mechanical Interaction (PCMI) due to the thermal expansion of the pellet. Experimental data from previous experiments in research reactor programs simulating RIAs show that at high burnup of the fuel in PWRs, the cladding undergoes a multiaxial loading state characterized by a strain biaxiality ratio $\varepsilon_{zz}/\varepsilon_{\theta\theta}$ between plane-strain (no axial strain in the cladding tube) and equal-biaxial tension (equal tensile strains in the hoop and axial directions). These values were obtained from measurements of the residual axial and hoop strain components on cladding tubes during CABRI REP-Na tests (3). These tests quantified the failure modes of rods during the first phase of a RIA transient, that of pellet-clad mechanical interaction (PCMI) in the temperature range of 600 °C.

To accurately reproduce the PCMI, a laboratory test should provide an appropriate strain rate with a displacement-controlled load, at the relevant test temperature, and with appropriate strain biaxiality.

The biaxiality of the strain components can have an important effect on the failure strain of a material. The effect of strain biaxiality on the strain at fracture has been reviewed by Yunchang and Koss (4) on unirradiated recrystallized Zircaloy-2 sheets. For cladding materials, the effect of biaxiality has been studied by many authors with different loading modes. Internal pressure tests have been used by Kaplar et al (5) to examine the impact of biaxiality in plane strain and equibiaxial conditions for unirradiated and irradiated Zr-1%Nb with low strain rates. Very few mechanical tests can load tubular samples with a high-biaxiality mechanical displacement-controlled load. The plane strain tensile test (PST) (6) and the magneto-forming test (7) can produce plane-strain and equibiaxial-strain conditions, respectively. However, the strain fields produced during these tests are heterogeneous, and interpretation of the results is difficult.

One of the tests that best represents PCMI involves placing a pellet-shaped cylindrical device inside a sample of fuel cladding. The device is compressed axially, causing it to expand in diameter, and thereby creating a hoop strain in the cladding sample. Mishima (8) developed a test in which a ductile, pellet-shaped lead cylinder was compressed by two pistons to measure the failure hoop strain of beryllium cladding tubes. Researchers have also used a segmented expanding mandrel with an axial core of ductile material, in order to simulate PCMI for stress

corrosion cracking tests (9). Compression of the ductile core causes the segmented mandrel to expand, thereby imposing a hoop strain on the sample. Expansion Due to Compression (EDC) tests have been the subject of various recent studies (10) - (16) due to its ability to characterize the failure mode encountered during the PCMI stage of RIAs.

In the original version of the EDC test, the ends of the tubular sample were free and unconstrained. During this type of free-end EDC test, the sample shrinks axially as it expands in diameter. Therefore, the strain biaxiality in the sample, $\varepsilon_{zz}/\varepsilon_{\theta\theta}$, is not representative of that experienced by fuel cladding during PCMI. In order to produce a more representative biaxial strain state in the sample, Nobrega (17) introduced a fixture to restrain the tube from axial shrinkage. The end restraining fixture prevents any change in length of the sample, so the strain biaxiality is much more representative than that of a free-end test. Hellouin de Menibus et al (18) used this type of fixed-end EDC test to study the effects of hydride blisters on the fracture of Zircaloy-4 cladding. They found that the fracture strain for a fixed-end EDC test is less than 50% of that of a free-end EDC test on unhydrided or hydrided samples at 25°C.

Shinozaki et al (19) (20) developed a type of EDC test in which the sample experiences tensile axial strain as well as tensile hoop strain. In this test, an axial tensile load is applied to the ends of the tubular sample as the ductile media is compressed inside the sample to control the biaxiality. Their study focused on pre-cracked specimens and showed that the hoop strain at failure tended to decrease as the strain biaxiality increased.

The objective of the current study is to examine the strain at failure obtained from EDC tests with different strain biaxiality ratios. Free-end EDC tests produce a state of nearly plane-stress in the sample, accompanied by a compressive axial strain. Fixed-end EDC tests produce a state of nearly plane-strain loading, in which the sample length is fixed. EDC tests with a tensile axial load produce tensile axial and hoop strains in the sample, and are the most representative of PCMI. Each method is used to test CWSR Zircaloy-4 samples. The objective is to study the effect of the strain biaxiality on the hoop strain at failure. In this study, the tests are performed at room temperature with strain rates on the order of 10^{-4}/s. Future efforts will focus on performing similar tests in more representative reactor conditions, at higher temperatures and with greater strain rates. The strain field in each sample is measured by a 3-dimensional DIC (Digital Image Correlation) technique, and the interpretation of the tests is supported by Finite Element Analysis (FEA).

This paper is organized as follows. In Section 2, the three configurations of EDC tests are presented, and the biaxiality of each test is discussed. Section 3 is devoted to the experimental procedure and the tests conditions and the experimental results for each test. FEAs of the EDC tests are presented in Section 4, and the simulated and experimentally measured strains are compared. Finally, some concluding remarks are presented in Section 5.

2. Experimental methods

The samples used in this study were non-irradiated Cold-Worked Stress Relieved (CWSR) Zircaloy-4 fuel cladding. The length, the outer diameter and the wall thickness of the sample are 27 mm, 9.5 mm, and 0.57 mm, respectively. The pellet inside the sample is made of Polytetrafluoroethylene (PTFE) and has a length of 14 mm and a diameter of 8.28 mm.

2.1 Free-end EDC test

The free-end EDC test consists of axially compressing, between two pistons, a ductile pellet inside a sample of cladding tube with free ends. The axial compression causes the pellet to expand in diameter, thereby creating a hoop strain in the cladding. This type of test reproduces the loading mode of PCMI, in which the expanding fuel pellet imposes a displacement-controlled strain on the fuel cladding. The tests can be performed at strain rates of the same order of magnitude as those experienced by the cladding during a RIA, typically $1.s^{-1}$. The EDC test also loads the cladding homogenously in the gauge section and gives conclusive results regarding crack profile (14).

The stress and strain biaxiality achieved in the free-end EDC test are close to uniaxial hoop tension. At the beginning of the test, the applied loading represents a state of plane stress, and the sample shrinks axially as it expands in diameter: $\varepsilon_{zz}/\varepsilon_{\theta\theta} = 0.6$ and $\sigma_{zz}/\sigma_{zz} = 0$. Thus,

the free-end EDC test does not accurately reproduce the stress and strain biaxiality conditions of PCMI.

The EDC test is performed using a force inverser on a tensile testing machine. Two pistons mounted on the force inverser pass inside the sample to compress the PTFE pellet. The design of the inversor device used to induce a compressive loading from a tensile testing machine is shown in Fig. 1-a.

2.2   Fixed-end EDC test

The fixed-end EDC test produces nearly plane strain conditions in the sample. In this test, stainless steel disks are inserted on either side of the pellet. A plug is then welded to each end of the sample. Each plug contains a central hole so that a piston can pass through it in order to compress the pellet. The outer end of the plug is threaded so that it can be connected to an end restraining fixture, as shown in Fig. 1-b. During the experiment, the length of the specimen does not change. Nevertheless, noteworthy negative local axial strain is obtained due to the friction between the pellet and the cladding. The plane strain condition is achieved only after significant piston displacement, when the circumferential strain becomes predominant.
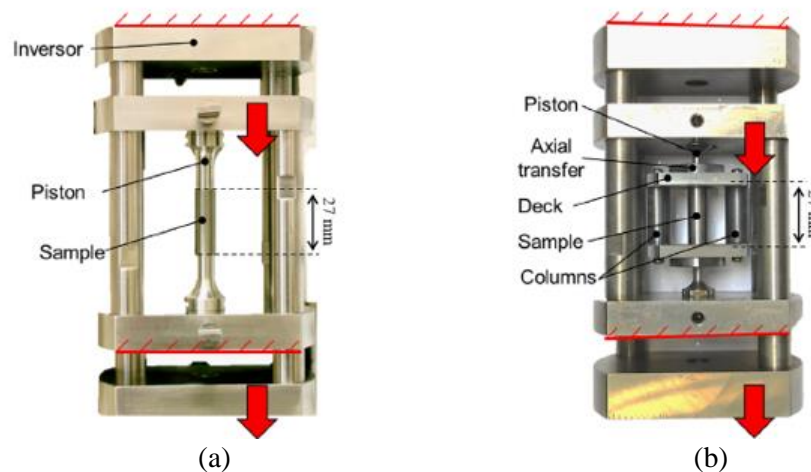

Fig. 1. Free-end EDC test geometry (a), Fixed-end EDC test geometry (b)

2.3   EDC test with a tensile load

A type of EDC test with an axial tensile load on the sample was developed in this study. Figure 2 presents a schematic illustration of the test. The test uses the same sample, with the same pellet and threaded end caps, described above for the fixed-end EDC tests. The tests are performed on a standard tensile testing machine using a special force inverser. The PTFE pellet in the cladding is compressed in the axial direction by two pistons, which are attached to the inner plates of the force inverser. The axial compression and subsequent diametrical expansion of the pellet lead to a tensile hoop strain in the sample. At the same time, four deformable tie rods (two on each side), which are attached to the outer plates of the force inverser, apply a tensile load to the ends of the sample. Therefore, the sample is subjected to tensile hoop and axial strains during the test.

The strain biaxiality, $\varepsilon_{zz}/\varepsilon_{\theta\theta}$, in this test is controlled by the mechanical behavior of the tie rods. These tie rods are made of stainless steel and are designed to deform plastically during the test. The force that they apply to the sample varies throughout the test and is a function of their geometry and the mechanical tensile behavior of the stainless steel, namely the yield strength and strain hardening characteristics. The dimensions of the ties rods must be determined by finite element modeling (FEM) in order to achieve the desired strain biaxiality. In this case, each tie rod was composed of 304L stainless steel and had an effective length of 60 mm and a cross sectional area of 20 mm^2. The simulations indicated that this configuration should lead to a strain biaxiality ratio $\varepsilon_{zz}/\varepsilon_{\theta\theta}$ of approximately 0.4.
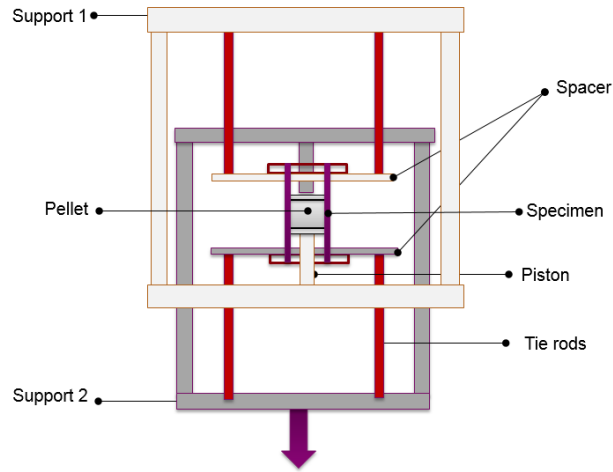
Fig. 2. EDC test with a tensile load

2.4 Measurements

All of the tests were performed on a MTS hydraulic tensile testing machine equipped with a 100 kN load cell. A computer recorded the applied load and the crosshead displacement as a function of time. The tests were performed at ambient temperature using a cross-head speed of 4 µm/s, inducing a hoop strain in the sample with a rate on the order of 10^{-4}/s. The strain field on the outer surface of the tube was measured by two cameras, as shown in Fig. 3, which are integrated with a 3D Digital Image Correlation (DIC) measurement system. Before performing the test, the face of the sample is painted with a speckled pattern. The stereo-correlation method is based on the principle of triangulation and maps the displacement field of the paint specks in 3D as a function of time. This technique provides the full-field 3-dimensional measurement of shape, displacement, and strain of the front face of the sample. Using this method, the Lagrangian strain tensor is available at every point on the specimen's front surface.
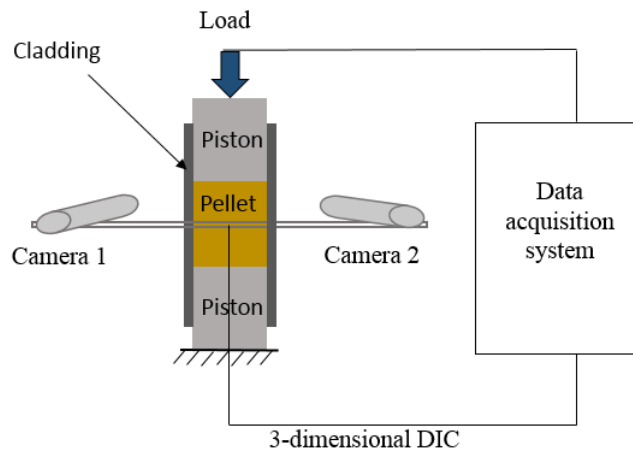

Fig. 3. Schematic representation of the EDC test setup and the 3D DIC

3 Experimental results

The experimental data for the three tests are presented in Figures 4. Each figure presents the force applied by the tensile testing machine and the measured axial and hoop strains in the central portion of the sample, as a function of the displacement of the cross head. Fig. 4(a) corresponds to the free-end EDC test. In this test, the sample did not rupture after 13 mm of cross head displacement. The central portion of the sample reached a hoop strain of 40% and an axial strain of -20%, but the sample did not rupture. Fig. 4(b) shows the results of the fixed-end EDC test. In this test, the sample failed at a hoop strain of 13% and an axial strain of -1%.

Fig. 4(c) shows the results of the EDC test with a tensile load. In this test, the sample failed at a hoop strain of 9% and an axial strain of 3.5%.
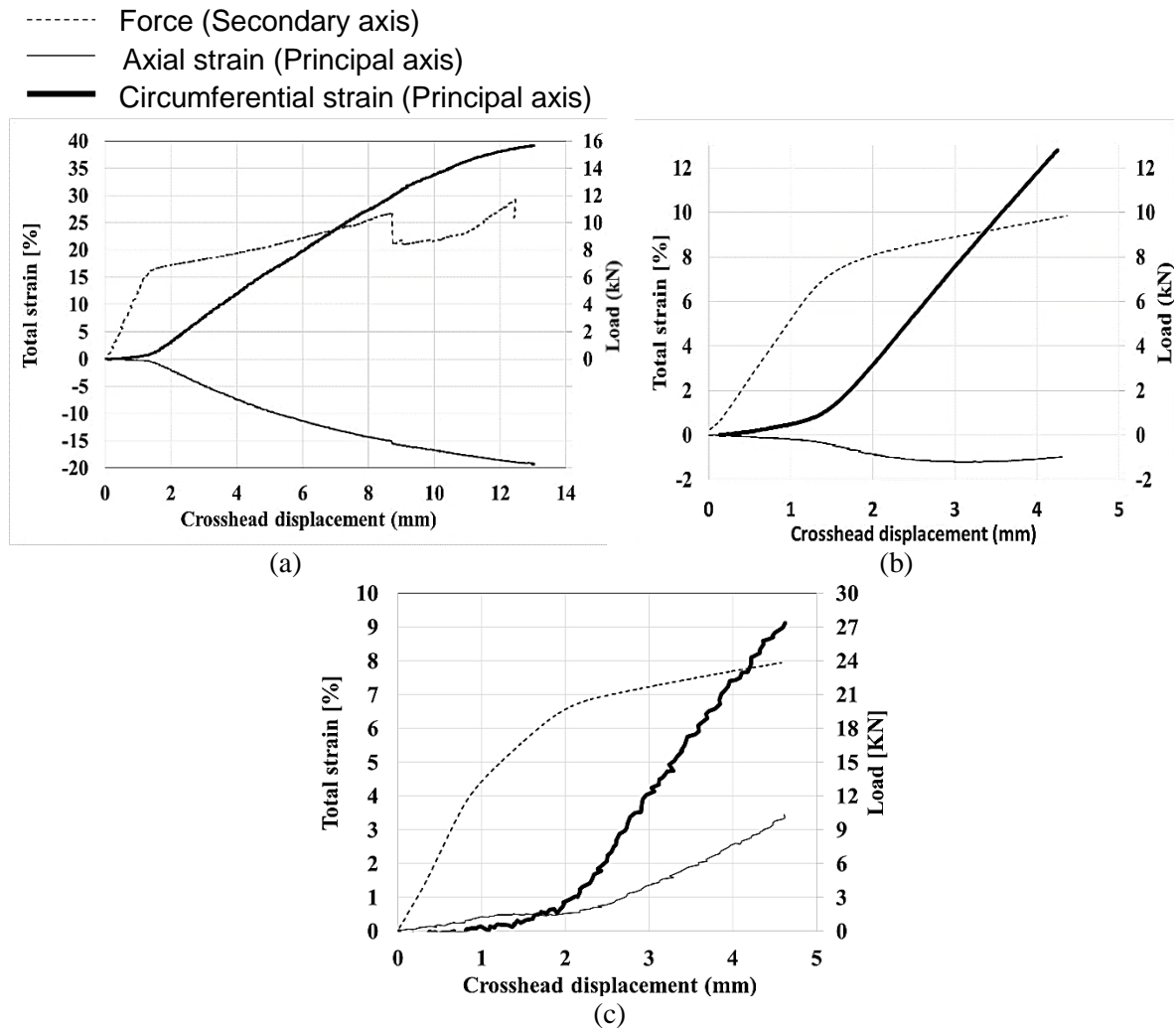

Fig. 4. Experimentally measured load-displacement curves and strain histories for free-end test (a), fixed-end test (b), and EDC test with a tensile load (c)

The boundary conditions greatly affect the strain biaxiality ratio $\varepsilon_{zz}/\varepsilon_{\theta\theta}$ produced in the three types of tests. The path of strain ratio for each configuration is shown in Fig. 5. The strain biaxiality ratio during the free-end EDC test is close to that of uniaxial tension. At the beginning of the test, the strain ratio is -0.6 and it increases to -0.5 after 40% circumferential strain.

For the fixed-end EDC test, the strain ratio is initially -0.3, and it increases to -0.07 at a hoop strain of 13%. Due to the friction between the pellet and the sample, an axial strain of approximately -1% is produced in the sample. At the end of this test, the strain ratio is -0.07 which is very close to a condition of plane strain.

For the EDC test with a tensile load, the tie rods produced a strain ratio close to 0.3, which is similar to the values measured in the CABRI REP-Na and NSRR HBO experiments. The strain ratio assessed during REP-NA3 is approximately 0.26 for Fuel burn-up of 54 MWd$(kgHM)^{-1}$ with a pulse width of 9.5 ms (21). Therefore, this study has shown that an EDC test with a tensile load is able to produce a strain biaxiality ratio close to that of the integrated RIA tests. The tie rods could be designed to produce values of strain biaxiality closer to 1, which will be the subject of future work.
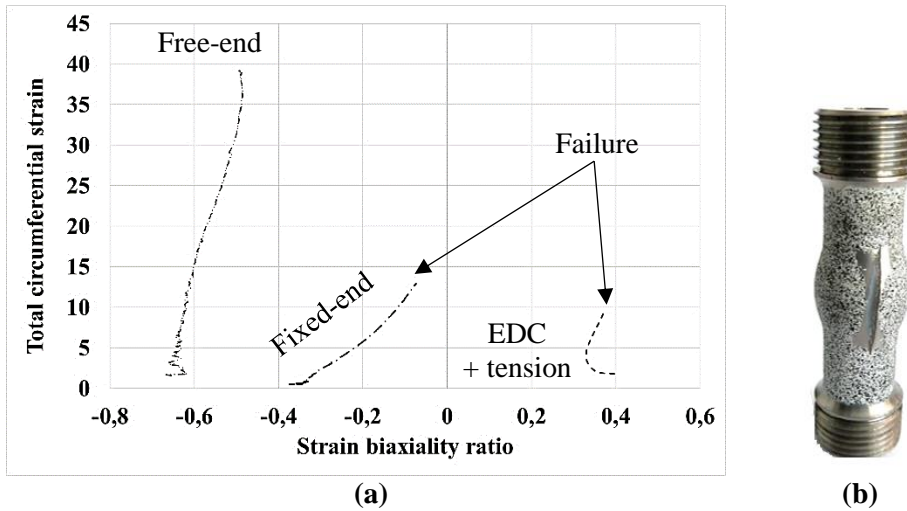
Fig. 5. Evolution of strain ratio for free-end, fixed end, and EDC with tensile load (a), failed sample after a fixed-end EDC test (b)

4   Numerical simulation

4.1   Simulation technique

FEA simulations of the EDC tests were performed using the Cast3M code, which was developed by the CEA (22). These simulations provide insight into the deformation and the failure modes observed during the tests. Quadrangular quadratic finite elements are used for the calculations, based on a large displacements and large rotations formulation. The geometry used for the finite element simulations of the EDC tests with a tensile load is shown in Fig. 6, along with the boundary conditions. In order to simplify the calculations, only half of the pellet and the cladding was modeled, as was done by previous researchers (8-12). The left edge of the model is the axis of rotation and is constrained in the radial (horizontal) direction. The bottom edge of the model is a plane of symmetry at the mid-plane of the sample and is constrained in the axial (vertical) direction. The tie rods are modeled as a single cylindrical structure with an appropriate cross-sectional area. The bottom surface of the tie rod is fixed to the upper surface of the fuel cladding. During the simulation, an axial (vertical) displacement is applied to the upper surface of the tie rod. This displacement is of the same magnitude but opposite direction as the displacement applied to the upper surface of the piston that compresses the pellet. Both the tie rod and the fuel cladding experience axial tensile plastic deformation as a result of this load, and at the same time, the pellet expands as it is compressed to apply a tensile hoop strain to the cladding.

The simulations of the fixed-end and free-end EDC tests use this same geometry, but without the tie rods. For the free-end EDC simulations, the top surface of the cladding tube is free and unconstrained. For the fixed-end EDC simulations, the top surface of the cladding tube is constrained in the axial (vertical) direction.
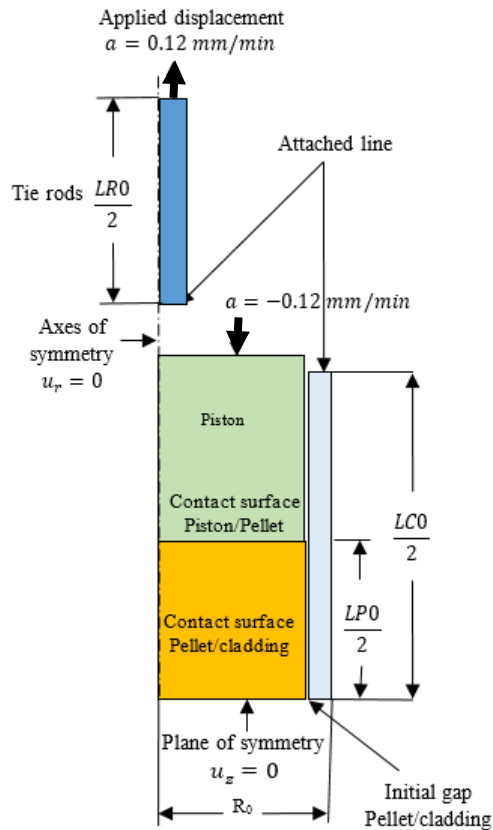
6

Fig. 6. Geometry and boundary conditions used for the finite element simulation of the EDC tests

In all of the simulations and experiments, there is an initial radial gap of 0.035 mm between the cladding and the pellet.

4.2 Material behavior

The mechanical behavior of the polymer pellet was calculated by analyzing compression tests, which were performed at CEA (18). An elastic isotropic model was chosen for the elastic phase, as well as a plastic isotropic model with linear isotropic strain hardening for the plastic phase.
An anisotropic plastic behavior law for the cladding tube that was specifically identified in RIA-PCMI conditions by Le Saux et al. (23) was used. Tensile tests were performed to identify the behavior of the 304L steel used for the tie rods (Fig. 7). Finite element simulations were then used to choose the cross section and the length of the rods.
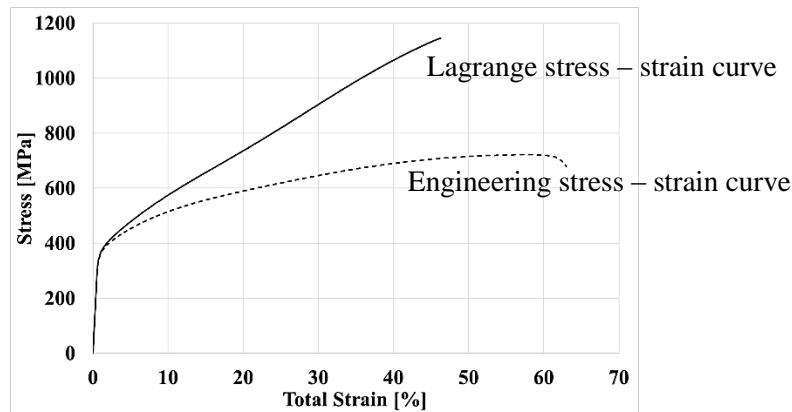

Fig. 7. Stress-strain curve for the 304L steel

4.3   Results and comparison with experiments

The coefficient of friction between the pistons and the pellet, μ_{PC}, has little influence on the simulated force-displacement response or on the local deformation of the specimen. However, the coefficient of friction between the pellet and the cladding, μ_{PC}, has an important effect on the simulated strain field, strain biaxiality, and force-displacement response. A wide range of values for the static and dynamic coefficients of friction between PTFE and steel have been reported in the literature. The current study assumes that the coefficient of friction between PTFE and zircaloy-4 is similar to that of PTFE and steel. Values in the range of 0.1 to 0.2 are common (12) (18) (24), but researchers have also reported values as large as 0.4 (25). It appears that the experimental method and the test conditions can have a significant effect on the measured coefficient of friction. In the current study, simulations were performed using values of 0.1, 0.2, and 0.4.

The experimentally measured hoop and axial strains are compared to the results of the simulations in Fig. 8. The values were taken at the mid-plane of the sample. The figure presents the strains calculated in the simulations for coefficients of friction of 0.1, 0.2, and 0.4. The figure indicates that the coefficient of friction between the pellet and the cladding has little influence on the circumferential strain for all of the types of tests considered. In addition, the graphs indicate a close agreement between the hoop strain values calculated in the simulations and those obtained experimentally from DIC measurements. On the other hand, the figure indicates that the coefficient of friction between the pellet and the cladding has an important effect on the axial strain. For the simulations of the free-end EDC test, increasing the coefficient of friction leads to increased axial shrinkage of the sample. The simulations were stopped after 7 mm of piston displacement because of a convergence problem. The same is true for the fixed-end EDC test, in which a greater coefficient of friction leads to larger negative axial strain in the sample. Likewise for the EDC test with a tensile load, in which the axial strain decreases as the coefficient of friction increases.

A coefficient of friction of 0.4 leads to the closest agreement between the simulations and the experimental results for the types of EDC tests considered. It is interesting to note that Desquines et al (26) used a value of 0.4 for the coefficient of friction between the pellet and the cladding in their simulations.
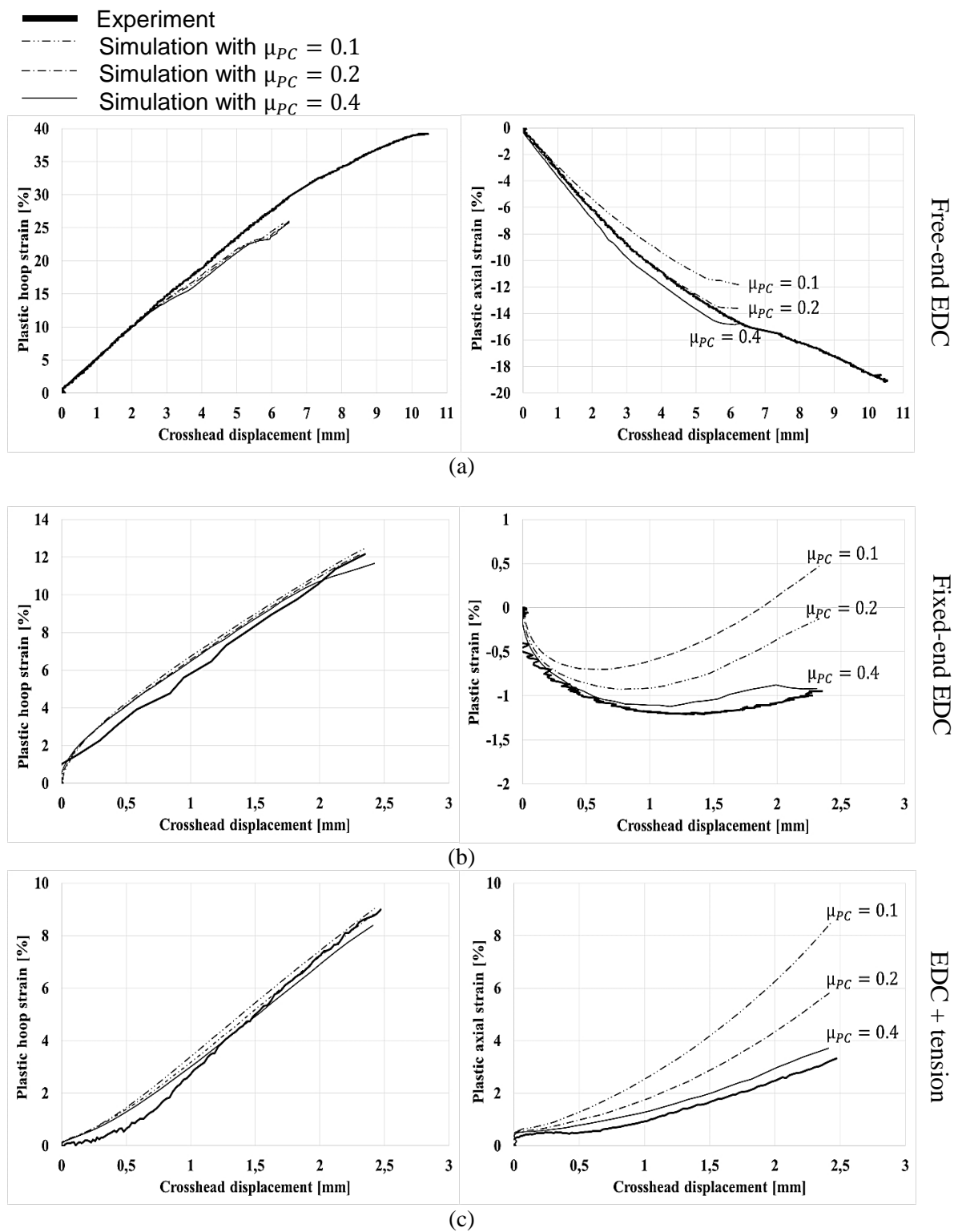
Fig. 8. Influence of the coefficient of friction μ_{PC} on axial and circumferential strains for free-end EDC test (a), fixed-end EDC test (b), and EDC test with a tensile load (c)

9

Conclusion

During a Reactivity-Initiated Accident (RIA), nuclear fuel cladding experiences a multiaxial loading state in which the Pellet-Cladding Mechanical Interaction (PCMI) produces a strain biaxiality ratio $\varepsilon_{zz}/\varepsilon_{\theta\theta}$ of between 0 and 1. This study investigates the effect of the strain biaxiality ratio on the hoop strain at failure of CWSR Zircaloy-4 fuel cladding samples. Experiments and simulations were performed for three types of Expansion Due to Compression (EDC) tests with different strain biaxiality ratios. Free-end EDC tests produce a state of nearly plane-stress in the sample, accompanied by a compressive axial strain. The strain biaxiality is not representative PCMI, and the sample did not failed at a hoop strain of 40%. Fixed-end EDC tests produce a state of nearly plane-strain loading, which is close to that of PCMI. This sample failed at a hoop strain of 13%. EDC tests with a tensile axial load produce tensile axial and hoop strains in the sample, and are the most representative of PCMI. In the current study, a test performed with a strain biaxiality ratio of 0.3 led to sample failure at a hoop strain of 9%. Thus, the tests show that the hoop strain at failure tends to decrease as the strain biaxiality ratio increases. The experimentally measured hoop and axial strains are in close agreement with Finite Element Analyses (FEA).

References

1. **J. Kima, M. Lee, Y. Jeong, J. Lim.** *Behavior of zirconium fuel cladding under fast pressurization rates. s.l. : Nuclear Engineering and Design , 2008, Vol. 238 1441–1447.*
2. **K. Yueh, J. Karlsson, J. Stjarnsater, D. Schrire, G. Ledergerber, C. Munoz-Reja, L. Hallstadius.** *Fuel cladding behavior under rapid loading conditions, s.l. : Journal of Nuclear Materials, 2006, Vol. 469 177-186.*
3. **J. Papin, B. Cazalis, J. M. Frizonnet, J. Desquines, F. Petit.** *Summary and Interpretation of the CABRI REP-Na Program.* 2007, Nuclear Technology, pp. 230-250.
4. **F.Yunchang, D. A. Koss.** *The Influence of Multiaxial States of Stress on the Hydrogen Embrittlement of Zirconium Alloy Sheet.* 1985. Metall.Trans. Vol. A16 675-681.
5. **E. Kaplar, L. Yegorova, K. Lioutov, A. Konobeyev, N. Jouravkova.** *Mechanical Properties of Unirradiated and Irradiated Zr-1% Nb Cladding.* s.l. : U.S. Nuclear Regulatory Commission, 2001.
6. **B. Cazalis, J. Desquines, S. Carassou, T. Le Jolu, C. Bernaudat.** *The plane strain tests in the PROMETRA program.* 127-142, s.l. : Journal of Nuclear Materials, 2016, Vol. 472.
7. **M. Leroy, A. Parrot, S. Leclercq.** *Failure characteristics of cladding tubes under RIA conditions through electromagnetic forming.* Toronto : s.n., 2007. Transactions, SMiRT 19.
8. **Mishima, Yoshitsugu.** *An Improved Testing Device for Measuring Tangential Expandability of Beryllium Tube.* 1966, Journal of Nuclear Science and Technology , pp. 294-297.
9. **Garlick, A.** *Frecture of zircaloy cladding under simulated power ramp conditions.* 1973, Journal of nuclear materials, pp. 209-224.
10. **Grigoriev, V., Jakobsson, R. and Schrire, D.** *Conditions, Experimental Evaluation of Critical Strain Energy Density for Irradiated Cladding under Simulated RIA.* 2001, Proceedings of ENS Topfuel 2001 Stockholm, Sweden.

11. **O. Dufourneaud, A.G. Varias, V. Grigoriev, R. Jakobsson and D.Schrire.** *Numerical simulation of the expansion due to compression test.* Tokai, Japan : s.n., 2001. Fuel Safety Research Specialists' Meeting.

12. **O. Dufourneaud, A. G. Varias.** *Elastic-Plastic Deformation of a Nuclear Fuel Cladding Specimen under the Internal Pressure of a Polymer Pellet.* Vienna, Austria : s.n., 2002. WCCM V Fifth World Congress on Computational Mechanics.

13. **Ménager, A. G. Varias** *Effect of External Hydride Layer on Fuel-Cladding Deformation during EDC Testing,.* **Y..** Prague, Czech Republic : s.n., 2003. Proc. of the 17th International Conference on Structural Mechanics in Reactor Technology (SMiRT 17).

14. **M. Le Saux, C. Poussard, X. Averty C. Sainte Catherine S. Carassou , J. Besson.** *High Temperature Expansion Due to Compression Test for the Determination of a Cladding Material Failure.* San Francisco, California : s.n., 2007. Proceedings of the 2007 International LWR Fuel Performance Meeting.

15. **F. Latourte, N. Rupin, M. He, A. Parrot, S. Leclercq.** *Full field measurements used for assessing industrial issues - Two examples.* 2012. Procedia IUTAM 4 .

16. **P. Magnusson, A. Alvarez-Holston, K. Ammon, G. Ledergerber, M. Nilsson, D. Schrire, K. Nissen, J. Wright.** *Effects of Zr-hydride distribution of irradiated Zircaloy-2 cladding in RIA-simulating pellet-clad mechanical interaction testing.* 246-252, s.l. : Nuclear Engineering and Technology, 2018, Vol. 50.

17. **B.N. Nobrega, J.S. king and G.S. was.** *Improvements in the design and analysis of the segmented expanding mandrel test.* 1985, journal of Nuclear Materials, Vol. 131, pp. 99-104.

18. **A. H. Menibus, Q. Auzoux, P. Mongabure, V. Macdonald, T. Le Jolu, J. Besson, J. Crépin.** *Fracture of Zircaloy-4 cladding tubes with or without hydride blisters in uniaxial to plane strain conditions with standard and optimized expansion due to compression tests.* s.l. : Materials Science and Engineering, 2014.

19. **T. Shinozaki, T. Mihara, Y. Udagawa, T. Sugiyama, M. Amaya.** *Failure Behavior of the Cladding with Outer Surface Pre-crack in Biaxial Stress Test.* 14-17, Sendai, Japan : Proceedings of WRFPM 2014 , 2014.

20. **T. Shinozaki, Y. Udagawa, T. Mihara, T. Sugiyama, M. Amaya.** *Improved-EDC tests on the Zircaloy-□ cladding tube with an outer surface pre-crack.* s.l. : Journal of nuclear science and technology, 2016.

21. **NEA.** *Nuclear fuel behaviour under reactivity-initiated accident (RIA) conditions.* 2010, OECD.

22. *http///www-cast3m.cea.fr.*

23. *M. Le Saux, J. Besson, S. Carassou, C. Poussard, X. Averty. A model to describe the anisotropic viscoplastic mechanical behavior of fresh and irradiated Zircaloy-4 fuel claddings under RIA loading conditions. 2008, Journal of Nuclear Materials, Vol. 379, pp. 60-69.*

24. *M.Dostál, M.Valach, J.Zymák. Extension of parametric calculations of the expansion due to compression test using fem model. s.l. : Water Reactor Fuel Performance Meeting, hengdu, China, Sept. 11-14, 2011 T3-032, 2011.*

25. *Biswas, S. K. Changes to near-surface region of PTFE during dry sliding against steel. s.l. : Journal of materials sciences , 1980, Vol. 1877-1885.*

26. *J. Desquines, D.A. Koss, A.T. Motta, B. Cazalis, M. Petit. The issue of stress state during mechanical tests to assess cladding performance during a reactivity-initiated accident (RIA). 250–267, s.l. : Journal of Nuclear Materials, 2011, Vol. 412.*